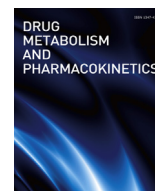




Contents lists available at ScienceDirect

Drug Metabolism and Pharmacokinetics

journal homepage: <http://www.journals.elsevier.com/drug-metabolism-and-pharmacokinetics>

Regular Article

Functional characterization of 9 CYP2A13 allelic variants by assessment of nicotine C-oxidation and coumarin 7-hydroxylation[☆]Q6 Masaki Kumondai^a, Hiroki Hosono^a, Masamitsu Maekawa^b, Hiroaki Yamaguchi^b, Nariyasu Mano^b, Akifumi Oda^c, Noriyasu Hirasawa^a, Masahiro Hiratsuka^{a, b, d, *}^a Laboratory of Pharmacotherapy of Life-Style Related Diseases, Graduate School of Pharmaceutical Sciences, Tohoku University, Sendai, 980-8578, Japan^b Department of Pharmaceutical Sciences, Tohoku University Hospital, Sendai, 980-8574, Japan^c Faculty of Pharmacy, Meijo University, Nagoya, 468-8503, Japan^d Tohoku Medical Megabank Organization, Tohoku University, Sendai, 980-8575, Japan

ARTICLE INFO

Article history:

Received 20 August 2017

Received in revised form

1 November 2017

Accepted 13 November 2017

Available online xxx

Keywords:

Cytochrome P450

CYP2A13

Genetic polymorphisms

Nicotine

Coumarin

ABSTRACT

Cytochrome P450 2A13 (CYP2A13) is responsible for the metabolism of chemical compounds such as nicotine, coumarin, and tobacco-specific nitrosamine. Several of these compounds have been recognized as procarcinogens activated by CYP2A13. We recently showed that CYP2A13*2 contributes to inter-individual variations observed in bladder cancer susceptibility because CYP2A13*2 might cause a decrease in enzymatic activity. Other CYP2A13 allelic variants may also affect cancer susceptibility. In this study, we performed an *in vitro* analysis of the wild-type enzyme (CYP2A13.1) and 8 CYP2A13 allelic variants, using nicotine and coumarin as representative CYP2A13 substrates. These CYP2A13 variant proteins were heterologously expressed in 293FT cells, and the kinetic parameters of nicotine C-oxidation and coumarin 7-hydroxylation were estimated. The quantities of CYP2A13 holoenzymes in microsomal fractions extracted from 293FT cells were determined by measuring reduced carbon monoxide-difference spectra. The kinetic parameters for CYP2A13.3, CYP2A13.4, and CYP2A13.10 could not be determined because of low metabolite concentrations. Five other CYP2A13 variants (CYP2A13.2, CYP2A13.5, CYP2A13.6, CYP2A13.8, and CYP2A13.9) showed markedly reduced enzymatic activity toward both substrates. These findings provide insights into the mechanism underlying inter-individual differences observed in genotoxicity and cancer susceptibility.

© 2017 The Japanese Society for the Study of Xenobiotics. Published by Elsevier Ltd. All rights reserved.

Q2 1. Introduction

Cytochrome P450 (CYP) 2A13 is an enzyme involved in the metabolism of several substrates, including coumarin, as well as nicotine and tobacco-specific nitrosamines 4-(methylnitrosamino)-1-(3-pyridyl)-1-butanone (NNK) and *N'*-nitrosornicotine (NNN) (Fig. 1) [1–4]. CYP2A13 also contributes to the genotoxicity caused by metabolic activation of aflatoxins and NNK, which is a representative procarcinogen included in tobacco [5]. In A549 cell transfectants, CYP2A13 mediated NNK metabolism to induce γ -H2AX production, a sensitive marker of DNA adducts [6]. An aflatoxin-mediated increase

in DNA-damage-response protein expression was reported in BEAS-2B cells, which express CYP2A13 [7]. The CYP2A13 mRNA is highly expressed in lung and bladder tissues (approximately 20 and 5×10^{-5} copies/0.1 μ g RNA described as CYP2A13/GAPDH, respectively) [8]. In these tissues, bioactivation of procarcinogen caused by CYP2A13 had a much larger contribution to genotoxicity.

Several CYP2A13 genetic polymorphisms have been identified in Japanese and French Caucasian populations [9–11]. The frequency of CYP2A13*2, specifically, has been reported with a frequency of 4.8–7.3% in Japanese individuals [9,11,12]. The Arg257Cys substitution caused by mutations in CYP2A13*2 is located at the carboxyl end of the G helix, resulting in a 2–3-fold reduction in CYP2A13 enzymatic activity [13,14]. CYP2A13*2 was associated with a decreased incidence of lung adenocarcinoma in smokers [15]. We previously found that the presence of CYP2A13*2 was associated with a reduced risk for bladder cancer, given that it decreases DNA damage caused by CYP2A13 [12]. Therefore, the enzymatic activity of CYP2A13 plays an important role in cancer development.

[☆] This study was supported by grants from the Smoking Research Foundation and Japan Research Foundation for Clinical Pharmacology.

* Corresponding author. Laboratory of Pharmacotherapy of Life-Style Related Diseases, Graduate School of Pharmaceutical Sciences, Tohoku University, 6-3, Aoba, Aramaki, Aoba-ku, Sendai, 980-8578, Japan.

E-mail address: mhira@m.tohoku.ac.jp (M. Hiratsuka).

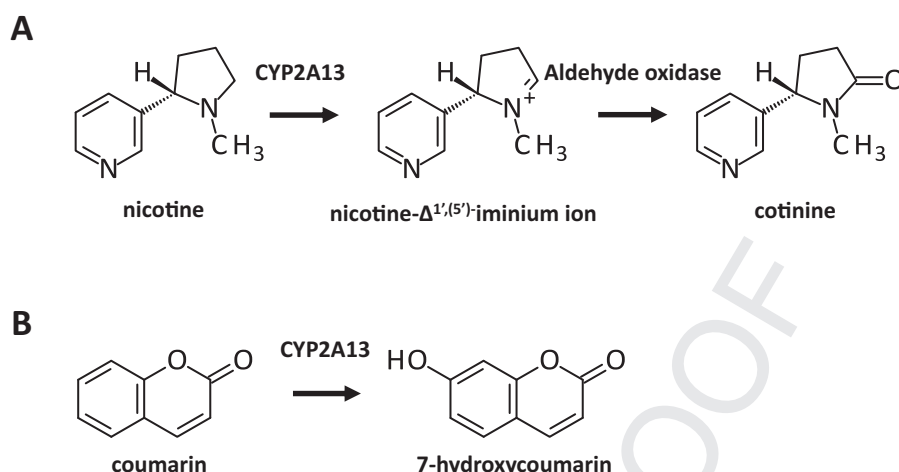


Fig. 1. Metabolic pathways from nicotine to cotinine catalyzed by CYP2A13 and aldehyde oxidase (A). Coumarin 7-hydroxylation metabolism catalyzed by CYP2A13 (B).

As shown in Table 1, several polymorphisms have been identified for the *CYP2A13* gene in addition to *CYP2A13**2 (<http://www.cypalleles.ki.se/cyp2a13.htm>) [Accessed Aug 9th, 2017]. The *in vitro* enzymatic activity of several of these variants has been characterized using a recombinant enzyme system such as *E. coli* cells [14,16,17]. Schlicht et al. reported that 3 substitutions (Asp158Glu, Arg257Cys, and Val323Leu) caused 2–3-fold decrease in enzymatic NNK α -hydroxylation activity [14]. *CYP2A13**4, which did not show an absorbance increase near 450 nm, did not have the ability to metabolize 5-methoxypsoralen [16]. These polymorphisms may affect individual variations in cancer development.

To characterize the currently known 8 *CYP2A13* variants, except for *CYP2A13**7, which contains an immature stop codon (Arg101-Stop) that causes the disappearance of enzymatic activity, we evaluated their activity using nicotine as a substrate, following protein expression in 293FT cells. In addition, coumarin 7-hydroxylation catalyzed by *CYP2A13* was measured to determine whether any functional changes observed were substrate-dependent.

2. Materials and methods

2.1. Chemicals

(–)-Nicotine, (–)-cotinine, (±)-cotinine-(methyl-d₃) derivatives, coumarin, 7-hydroxycoumarin, and 4-methyl-7-hydroxycoumarin were purchased from Sigma-Aldrich (Tokyo, Japan). The UltraPool Human Liver Cytosol, 150-Donor Pool was purchased from Corning Incorporated (Corning, NY, USA). Oxidized β -nicotinamide-adenine

Table 1
Cytochrome P450 2A13 (*CYP2A13*) allelic variants characterized in this study.

Variants	Protein	Nucleotide changes	Amino acid changes
<i>CYP2A13</i> *1	CYP2A13.1		
<i>CYP2A13</i> *2	CYP2A13.2	74G > A 3375C > T	Arg25Gln Arg257Cys
<i>CYP2A13</i> *3	CYP2A13.3	1634_1635insACC 1706C > T	133_134insThr Asp158Glu
<i>CYP2A13</i> *4	CYP2A13.4	579G > A	Arg101Gln
<i>CYP2A13</i> *5	CYP2A13.5	7343T > A	Phe453Tyr
<i>CYP2A13</i> *6	CYP2A13.6	7465C > T	Arg494Cys
<i>CYP2A13</i> *8	CYP2A13.8	1706C > T	Asp158Glu
<i>CYP2A13</i> *9	CYP2A13.9	5294G > T	Val323Leu
<i>CYP2A13</i> *10	CYP2A13.10	74G > A 3375C > T 5792T > C	Arg25Gln Arg257Cys Ile331Thr

dinucleotide phosphate oxidized form (NADP⁺), glucose-6-phosphate (G-6-P), glucose-6-phosphate dehydrogenase (G-6-PDH), and β -nicotinamide-adenine dinucleotide phosphate reduced form (NADPH) were purchased from Oriental Yeast (Tokyo, Japan). The following reagents were purchased from the indicated sources: polyclonal anti-human *CYP2A13* antibody (ab58740, Abcam, CB, UK); polyclonal anti-calnexin antibody (Enzo Life Sciences, Farmingdale, NY, USA); horseradish peroxidase (HRP)-conjugated goat anti-rabbit IgG (Santa Cruz Biotechnology, Santa Cruz, CA, USA). Triton N-101 and sodium cholate hydrate were obtained from Sigma-Aldrich. Sodium cyanide and cytochrome c from horse heart were purchased from Nacalai Tesque (Kyoto, Japan).

2.2. *CYP2A13* cDNA cloning and construction of expression vectors

Plasmids carrying full-length *CYP2A13* cDNA fragments (GenBank accession no. AF209774.1) were obtained from GenScript (USA). *CYP2A13* cDNA fragments from plasmid DNA were PCR-amplified using a forward primer (5'-CACCATGCTGGCCTCAGGGCTGCTTC-3') and a reverse primer (5'-TCAGCGGGCAGGAAGCTCATGGTGTAG-3') and *PfuUltra* High-Fidelity DNA Polymerase (Agilent Technologies, Santa Clara, CA, USA), the underlined sequence in the forward primer were introduced for directional TOPO cloning. Following amplification, the wild-type *CYP2A13* fragments were subcloned into the pENTR/D-TOPO vector (ThermoFisher Scientific, Waltham, MA). A plasmid containing *CYP2A13**1 cDNA was used as a template to generate various *CYP2A13* allelic variant constructs (*CYP2A13**2, *CYP2A13**4–*CYP2A13**6, *CYP2A13**8, and *CYP2A13**9), using the primer set for site-directed mutagenesis (Supplemental Table 1) and the QuikChange Site-directed Mutagenesis Kit (Stratagene, La Jolla, CA, USA) following the manufacturer's instructions. Other *CYP2A13* constructs were generated from plasmids carrying other cDNA templates: *CYP2A13**3 from *CYP2A13**8 cDNA, and *CYP2A13**10 from *CYP2A13**2 cDNA. All wild-type and variant cDNAs prepared were confirmed by Sanger sequencing. Wild-type and *CYP2A13* variant cDNAs were subcloned into the mammalian expression vector pcDNA3.4 (ThermoFisher Scientific).

2.3. Expression of *CYP2A13* variants in 293FT cells

293FT cells, purchased from ThermoFisher Scientific, were cultured in Dulbecco's modified Eagle's medium (Nacalai Tesque) containing 10% fetal bovine serum at 37 °C under 5% CO₂. Cells were transfected with a plasmid (5 μ g) encoding *CYP2A13* cDNA, using

the TransFectin lipid reagent (Bio-Rad Laboratories, Hercules, CA, USA) according to the manufacturer's instructions. After incubation for 24 h at 37 °C, the 293FT cells were scraped off, and the microsomal fractions were prepared as previously described. Protein concentrations were determined using the BCA Protein Assay Kit (ThermoFisher Scientific).

2.4. Determination of microsomal P450 contents

The concentrations of CYP2A13 variant holoenzymes were spectrophotometrically measured according to previously reported methods, with several modifications [18,19]. The microsomal fraction (approximately 1.5 mg of microsomal proteins) was diluted to 200 μL in 100 mM potassium phosphate buffer (pH 7.4) containing 1.0 mM EDTA, 20% glycerol (v/v), 0.5% sodium cholate (w/v), and 0.4% Triton N-101 (w/v). One hundred microliter of protein samples was added to sample and reference cuvettes. A baseline between 400 and 500 nm was recorded using a Cary 300 UV–Vis Spectrophotometer (Agilent Technologies). CO gas was bubbled through the mixture in the sample cuvette at a flow rate of 1 bubble/s for 20 s. Samples were reduced in the presence of approximately 0.2 mg of solid $\text{Na}_2\text{S}_2\text{O}_4$. The absorbance spectra of both cuvettes were then recorded between 400 and 500 nm using a spectrophotometer. The CO-difference spectra were recorded three times for each CYP2A13 variant. Data analysis was conducted using a Jasco Spectra Manager (JASCO Corporation, Sendai, Japan). The cytochrome P450 concentration was calculated using the maximum absorbance of three records normalized to the baseline spectrum because the spectrum baseline showed a difference in absorbance between 400 and 500 nm. Cuvettes (Sub-Micro Cells, 16.50-Q-10/Z20) were purchased from Starna Scientific, Ltd. (London, UK).

2.5. Western blot analysis

293FT microsomal fractions (5 μg microsomal protein) were separated by 10% sodium dodecyl sulfate-polyacrylamide gel electrophoresis (SDS-PAGE). Western blotting was performed according to standard procedures. CYP2A13 was detected using a polyclonal anti-human CYP2A13 antibody (diluted 1:5000). Calnexin was detected using a polyclonal anti-calnexin antibody (1:5000), as a loading control. Detection was achieved using a secondary HRP-conjugated goat anti-rabbit IgG (1:10,000). Western blots were visualized using SuperSignal West Dura Extended Duration Substrate (ThermoFisher Scientific). Chemiluminescence was quantified using a ChemiDoc XRS⁺ system with Image Lab Software (Bio-Rad Laboratories).

2.6. Measurement of NADPH-cytochrome c reduction activity

The activity of NADPH-cytochrome P450 reductase (CPR) was evaluated according to previous methods described by Omura and Takesue (1970) [20]. The microsomal fraction (100 μg of microsomal proteins) was diluted to 180 μL in 100 mM potassium phosphate buffer (pH 7.4) containing 1.0 mM sodium cyanide. Protein samples (90 μL) were added to sample and reference cuvettes. A blank was recorded at 550 nm using a Cary 300 UV–Vis spectrophotometer (Agilent Technologies). Reactions were initiated by addition of 1.0 mM NADPH diluted in 100 mM potassium phosphate buffer (pH 7.4) containing 1.0 mM sodium cyanide. The control sample contained all of the reagents except for NADPH in a reference cuvette. The absorbance was recorded for each microsomal fraction expressing CYP2A13 variant protein until the absorbance versus time plot was no longer linear. The activity of

CPR towards cytochrome c was calculated using the extinction coefficient of cytochrome c (21 mM^{-1} per cm at 550 nm).

2.7. Nicotine C-oxidation assay

CYP2A13 nicotine C-oxidation activity was determined as previously described methods, with several modifications [21,22]. The reaction mixture, in a total volume of 100 μL , consisted of the following: the microsomal fraction (20 μg), UltraPool Human Liver Cytosol, 150-Donor Pool as a source of aldehyde oxidase (10 μg), nicotine (0.5, 1, 2, 5, 10, 20, 50, or 100 μM), and 50 mM potassium phosphate buffer (pH 7.4). Following pre-incubation at 37 °C for 3 min, reactions were initiated by the addition of an NADPH-generating system, consisting of 0.5 mM NADP^+ , 5 mM G-6-P, 5 mM MgCl_2 , and 1 U/mL G-6-PDH, with incubation at 37 °C for 20 min. Reactions were terminated by adding 100 μL of acetonitrile containing 1 μM cotinine-(methyl-d3) as an internal standard. Determination of nicotine C-oxidation in 20 μg of the microsomal fraction (containing wild-type CYP2A13 and CYP2A13 variants) showed that cotinine formation was linear for incubations of up to 20 min. Moreover, when the reaction was performed for 20 min with 0–20 μg of microsomal protein, cotinine formation was linear in the presence of up to 20 μg of microsomal protein (data not shown).

After centrifuging the reaction tube at 15,400 \times g for 10 min, 150 μL of the supernatant was diluted twice using water. The resulting solution (10 μL) was injected into a liquid chromatography tandem mass spectrometry system, according to previously described methods [21,22]. Enzymatic activity was normalized to the amount of CYP2A13 holo-protein.

2.8. Coumarin 7-hydroxylation assay

CYP2A13-dependent coumarin 7-hydroxylation was measured as previously reported, with several modifications [22,23]. The reaction mixture (100 μL) contained the microsomal fraction (30 μg), coumarin (2, 4, 6, 8, 10, 15, or 20 μM), and 50 mM potassium phosphate buffer (pH 7.4). Following pre-incubation at 37 °C for 3 min, reactions were initiated by the addition of an NADPH-generating system (described above). After incubating at 37 °C for 10 min, reactions were terminated by adding 100 μL acetonitrile containing 200 nM 4-methyl-7-hydroxycoumarin as an internal standard. Coumarin 7-hydroxylation activity was determined in the microsomal fractions containing 1 of each CYP2A13 variant (30 μg of microsomal protein). Data obtained using coumarin revealed that 7-hydroxycoumarin formation was linear for incubations of up to 10 min. Under these conditions, the formation of 7-hydroxycoumarin was linear in the presence of up to 30 μg of microsomal protein (data not shown).

After centrifuging the reaction tube at 15,400 \times g for 10 min, 150 μL of the supernatant was diluted twice in 50 mM potassium phosphate buffer (pH 7.4) and 50 μL of the diluted solution was subjected to HPLC. Quantitative determination of 7-hydroxycoumarin was conducted as previously described [22,23]. The enzymatic activity was normalized to the amount of CYP2A13 holo-protein.

2.9. Data analysis

Kinetic data, including the K_m , maximum velocity (V_{max}), and intrinsic clearance ($CL_{int} = V_{max}/K_m$) values, were determined using the Enzyme Kinetics Module of SigmaPlot 12.5 (Systat Software, Inc., Chicago, IL, USA), a curve-fitting program based on nonlinear regression analysis. All values are expressed as the mean \pm SD of experiments performed in triplicate. Statistical analyses of enzymatic activity and kinetic parameters were performed through variance analysis by Dunnett's T3 test or the Kruskal–Wallis

method (IBM SPSS Statistics Ver. 22, International Business Machines, Armonk, NY, USA). Differences or correlations with $P < 0.05$ were considered statistically significant.

2.10. Three-dimensional (3D) structural modeling of CYP2A13

The 3D structural modeling of CYP2A13 was based on the CYP2A13 X-ray structure of DeVore et al. (2012) (Protein Data Bank code 3T3S) [24]. After removal of the substrate, nicotine or coumarin was docked with the CYP2A13 X-ray structure according to the CDOCKER protocol of Discovery Studio 2.5 (BIOVIA, CA, USA). Docking iterations were conducted taking into consideration the binding orientation and binding energies under the following conditions that the volume of the space was defined as 9 and the heme iron was charged to Fe^{3+} .

3. Results

The CYP2A13 protein levels in 293FT cells were assessed by Western blotting with a polyclonal CYP2A13 antibody. As shown in Fig. 2, CYP2A13 protein was detected for all variants, but not in the mock-treated cells. Calnexin, used as an endoplasmic reticulum-resident protein, showed constant expression levels in the microsomes of transfected cells.

We measured the reduced CO-difference spectra with the microsomal fractions for each CYP2A13 variant (1.66 ± 0.24 mg). We found an increase in the maximum absorption wavelength after CO treatment of wild-type CYP2A13 and 5 CYP2A13 variants (CYP2A13.2, CYP2A13.5, CYP2A13.6, CYP2A13.8, and CYP2A13.9). The results indicated the presence of functional CYP enzymes and the expression levels of CYP2A13 variants (Fig. 3). Three CYP2A13 variants (CYP2A13.3, CYP2A13.4, and CYP2A13.10) showed no increase in their absorption maxima at 450 nm.

We evaluated whether the CPR activity was different for each CYP2A13 variant. The CPR activity for the wild type was 25.2 ± 2.71 nmol min^{-1} mg protein $^{-1}$. For all CYP2A13 variants, there was no significant difference in CPR activity compared to that for the wild type enzyme (Supplemental Fig. 1).

The K_m , V_{max} , and CL_{int} values for nicotine C-oxidation by CYP2A13.1 were 4.60 μM , 31.5 pmol min^{-1} pmol $^{-1}$ CYP2A13, and 6.86 μL min^{-1} pmol $^{-1}$ CYP2A13, respectively (Table 2). The K_m values for CYP2A13.2, CYP2A13.5, CYP2A13.6, CYP2A13.8, and CYP2A13.9 were not significantly different from that of CYP2A13.1. For the 5 CYP2A13 variants (CYP2A13.2, CYP2A13.5, CYP2A13.6, CYP2A13.8, and CYP2A13.9), the V_{max} and CL_{int} values were significantly lower than that of CYP2A13.1. The K_m , V_{max} , and CL_{int} values for coumarin 7-hydroxylation by CYP2A13.1 were 2.34 μM , 442 fmol min^{-1} pmol $^{-1}$ CYP2A13, and 183 nL min^{-1} pmol $^{-1}$ CYP2A13, respectively. Relative to that of wild-type CYP2A13, the K_m values for CYP2A13.2, CYP2A13.5, and CYP2A13.8 were significantly higher. In contrast, the K_m value for CYP2A13.9 was significantly lower than that of wild-type CYP2A13. Relative to those of

wild-type CYP2A13, the V_{max} and CL_{int} values for the 5 CYP2A13 variants (CYP2A13.2, CYP2A13.5, CYP2A13.6, CYP2A13.8, and CYP2A13.9) were significantly lower. For 3 variants (CYP2A13.3, CYP2A13.4, and CYP2A13.10), the kinetic parameters could not be determined because nicotine C-oxidation and coumarin 7-hydroxylation activity were not detected.

4. Discussion

CYP2A13 is one of the most potent metabolic activators of NNK among human CYPs [1]. Nicotine and coumarin are also representative substrates metabolized by CYP2A13 [2–4]. CYP2A13 genetic polymorphisms can affect individual responses to these substrates, which may result in observed differences in smoking behavior and cancer risk. In this study, we characterized the enzymatic activity of 9 CYP2A13 variant alleles, using the variant proteins overexpressed in 293FT cells. We determined the kinetic parameters for wild-type and 5 CYP2A13 variants (CYP2A13.2, CYP2A13.5, CYP2A13.6, CYP2A13.8, and CYP2A13.9) in terms of nicotine C-oxidation and coumarin 7-hydroxylation. The results demonstrated that after CO-treatment, 3 CYP2A13 variant proteins (CYP2A13.3, CYP2A13.4, and CYP2A13.10) showed no increase in absorbance near 450 nm, reflecting failed heme incorporation.

The CL_{int} values obtained for nicotine C-oxidation versus those for coumarin 7-hydroxylation for CYP2A13.2, CYP2A13.5, and CYP2A13.8 indicated a high correlation. The Arg257Cys substitution located on the carboxyl-terminal end of the G helix caused a reduction in enzymatic activity. The repeating pattern of hydrophobic residues in the G helix is conserved in CYP2 families [25]. Lehnerer et al. (2000) reported that the Arg253Ala substitution, which is located near the end of the G helix, led to decreased enzymatic activity due to interference in the interaction between rabbit CYP2B4 and P450 reductase [26]. Therefore, a reduction in the binding between CYP2A13 and P450 reductase, caused by the Arg257Cys substitution, could reduce CYP2A13.2 activity. In contrast, the Arg25Glu substitution, present in CYP2A13.2 and located in the membrane anchor region, may not influence the enzymatic activity of CYP2A13 because the enzymatic activities for NNK α -hydroxylation and coumarin 7-hydroxylation were reduced in case of the Arg257Cys substitution [14]. CYP2A13.5, which contains a Phe453Tyr substitution, showed 20% less activity than CYP2A13.1 did. The Phe453 residue, located in the hydrophobic region of the L helix alongside Leu449, interacts with the distal I helix [25]. The Phe453Tyr substitution causes a conformational change in the K and I helices, which in turn causes a reduction in enzymatic activity. CYP2A13.8 has a substitution in residue Asp158 located in the D helix, which interacts with residues in the G and H loop. This interaction between the C/D and G/H loops could provide a physical coordination mechanism underlying the observed ligand-induced conformational changes in the electron-delivery system of the protein, located on the proximal side of the mammalian CYP2B6 structure [27]. As reported previously, the CYP2A6.2 variant with a Leu160His substitution located in the D helix, led to a loss of coumarin 7-hydroxylation activity [28]. In the case of CYP2A13.8, Asp158Glu could also cause interactions between the C/D and G/H loops. Thus, the reduced enzymatic activity of these variants may influence intra-individual differences found in cancer risk and genotoxicity.

Overall, all 8 CYP2A13 variants showed similar expression levels relative to the wild-type enzyme; however, CYP2A13.3, CYP2A13.4, and CYP2A13.10 were functionally inactive, despite showing expression levels comparable to that of the wild-type enzyme. In the case of CYP2A13.3, the addition of a Thr residue between 133Ala and 134Thr results from the insertion of 3 nucleotides in the carboxyl end of the C helix. Schlicht et al. (2007) reported that it

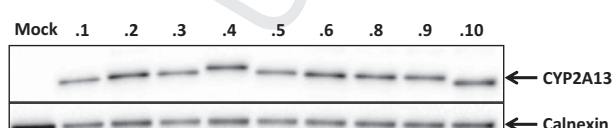


Fig. 2. Western blots showing immunoreactive CYP2A13 proteins (upper panel) and calnexin (lower panel). Western blotting was performed according to standard procedures using 10% SDS-PAGE. Five micrograms of microsomal fractions containing CYP2A13 variant proteins was loaded onto each lane. CYP2A13 variants and calnexin were detected using polyclonal antibodies against the respective proteins. The numbers correspond to each CYP2A13 variant.

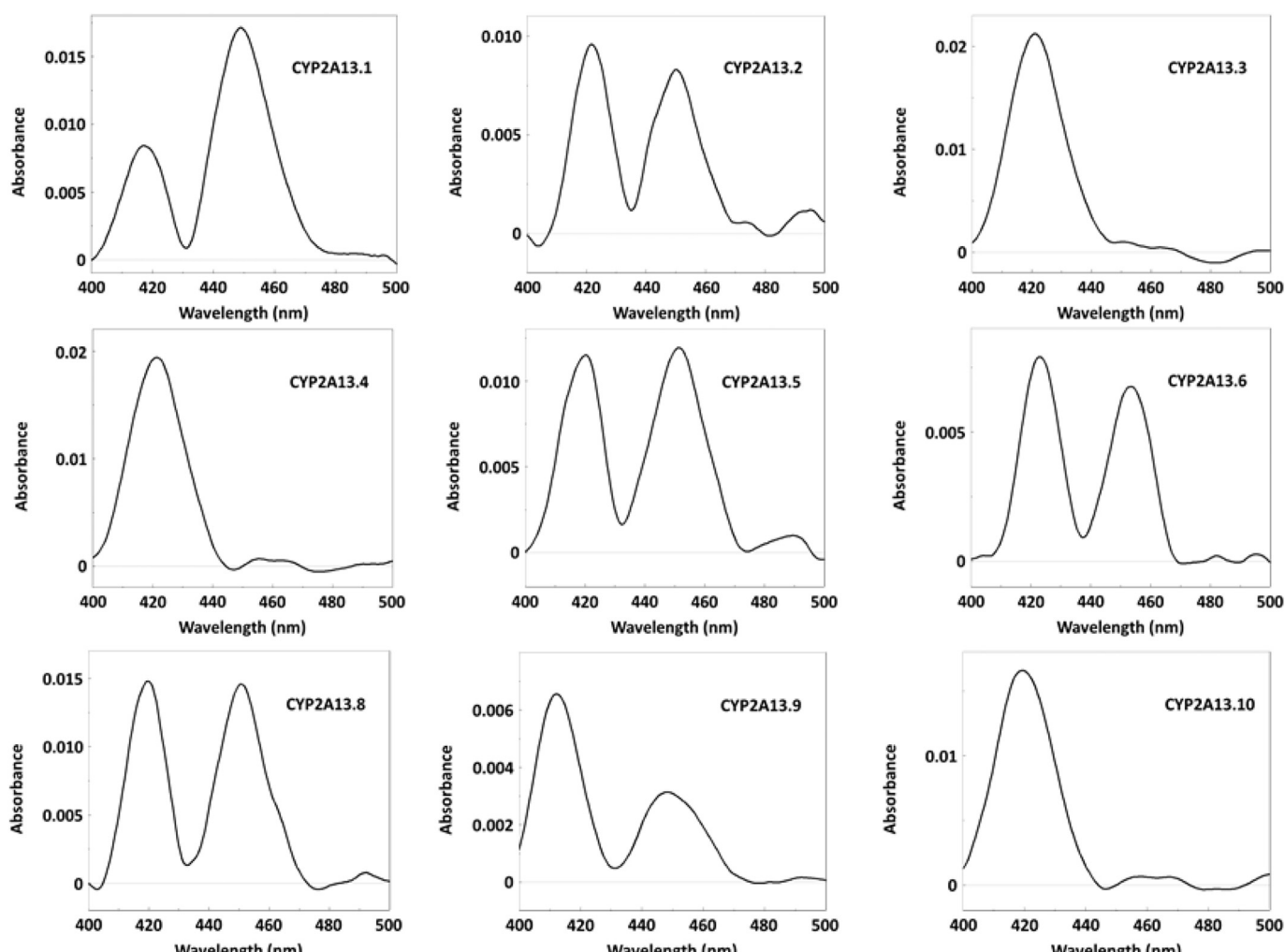


Fig. 3. CO-difference spectra of CYP2A13 proteins expressed in 293FT cells.

Table 2

Kinetic parameters of nicotine C-oxidation and coumarin 7-hydroxylation.

Variants	Nicotine C-oxidation			Coumarin 7-hydroxylation		
	K_m (μM)	V_{max} (pmol/min/pmol CYP2A13)	CL_{int} (V_{max}/K_m) ($\mu\text{L}/\text{min}/\text{pmol}$ CYP2A13) (% of wild-type)	K_m (μM)	V_{max} (fmol/min/pmol CYP2A13)	CL_{int} (V_{max}/K_m) (nL/min/pmol CYP2A13) (% of wild-type)
CYP2A13.1	4.60 \pm 0.32	31.5 \pm 1.79	6.86 \pm 0.10	2.34 \pm 0.06	442 \pm 12.7	183 \pm 4.91
CYP2A13.2	7.34 \pm 0.96	14.9 \pm 1.79***	2.07 \pm 0.50* (30%)	3.20 \pm 0.27*	191 \pm 7.00***	59.9 \pm 4.02*** (33%)
CYP2A13.3	N.D.	N.D.	N.D.	N.D.	N.D.	N.D.
CYP2A13.4	N.D.	N.D.	N.D.	N.D.	N.D.	N.D.
CYP2A13.5	6.43 \pm 0.49	5.98 \pm 0.42**	0.93 \pm 0.05*** (14%)	3.88 \pm 0.69***	127 \pm 10.1***	33.2 \pm 3.28*** (18%)
CYP2A13.6	10.9 \pm 1.84	15.4 \pm 1.62***	1.43 \pm 0.14*** (21%)	1.97 \pm 0.27	184 \pm 7.69***	94.3 \pm 8.37*** (52%)
CYP2A13.8	3.48 \pm 1.33	5.52 \pm 0.14**	1.78 \pm 0.76* (26%)	3.48 \pm 0.29**	120 \pm 4.83***	34.7 \pm 3.66*** (19%)
CYP2A13.9	20.8 \pm 13.1	16.9 \pm 5.11***	0.91 \pm 0.25** (13%)	1.35 \pm 0.10*	184 \pm 1.92***	137 \pm 10.2*** (75%)
CYP2A13.10	N.D.	N.D.	N.D.	N.D.	N.D.	N.D.

These data represent the mean \pm SD of three independently performed catalytic assays.

* $P < 0.05$, ** $P < 0.01$, and *** $P < 0.005$ compared to CYP2A13.1. N.D. represents not determined.

The kinetic parameters of nicotine C-oxidation of CYP2A13.3, CYP2A13.4, and CYP2A13.10 could not be determined because the enzymatic activity of CYP was not detected at the highest substrate concentration assayed (100 μM nicotine).

The kinetic parameters of CYP2A13.3, CYP2A13.4, and CYP2A13.10 could not be determined because the enzymatic activity of CYP was not detected at the highest substrate concentration assayed (20 μM coumarin).

was not possible to obtain the CYP2A13.3 protein in active form, due to degradation during purification [14]. In agreement with their findings, the protein instability of CYP2A13.3 prevented us from observing an increase in the maximum absorption wavelength at 450 nm CYP2A13.4 has a substitution in a heme pocket-

forming amino acid, in the substrate-recognition site-1, which causes a loss of catalytic activity and inappropriate heme binding in CYP2A13.4 prepared from Sf9 cells [16]. Our results also demonstrated a dramatic decrease in the enzymatic activity of CYP2A13.4 in a heterologous expression system using mammalian cells. This

decrease resulted from the decrease in CYP2A13 holo-protein levels caused by disruption of the interaction between Arg101 and heme (Fig. 4). CYP2A13*10 was identified in the Japanese population [11], although the catalytic efficiency of its protein product is still unknown. CYP2A13.10 has 3 nucleotide mutations leading to the Arg25Glu, Arg257Cys, and Ile331Thr substitutions. Ile331, located in the J helix of CYP2A13, may affect D-E loop formation. The negatively charged D-E loop region interacts with the positively charged heme-proximal cavity, which influences the electrostatic status of the neighboring active site heme [29]. The Ile331Thr substitution, found in CYP2A13.10, causes hydrogen bond formation between Thr331 and Cys494, and then the conformation of the D-E loop region is dramatically changed (Fig. 5). This conformational change may influence the stability of the CYP2A13 holo-protein. The decreased CYP2A13.10 stability caused by the Ile331Thr substitution (in addition to the Arg25Glu and Arg257Cys substitutions), leads to a complete loss of enzymatic activity. Therefore, CYP2A13.3, CYP2A13.4, and CYP2A13.10 also appear to contribute to a decreased risk of bladder cancer, since this risk was significantly decreased in individuals who harbor the CYP2A13*2 variant allele [12], which has been associated with reduced metabolic activity of tobacco-specific nitrosamines, including NNK.

The nicotine C-oxidation CL_{int} values for CYP2A13.6 and CYP2A13.9 decreased by 21% and 13% respectively, relative to that for wild-type CYP2A13, whereas coumarin 7-hydroxylation CL_{int} values decreased by 52% and 75% respectively, relative to that for wild-type CYP2A13. Arg494, located at the CYP2A13 carboxy-terminal domain, forms hydrogen bonds with His328, Asp332,

Met457, Asn459, and Phe460. The Arg494Cys substitution, found in CYP2A13.6, causes hydrogen bond formation between Cys494 and Lys337, while disrupting hydrogen bond formation between Arg494 and His328, and Asp332 and Phe460 (Fig. 6A). Several channels have been identified in bacterial, archaeal, and mammalian P450 enzymes [30]. A solvent channel, which could serve as a product exit channel, is located between the E and I helices and the β_5 sheet. No remarkable conformational changes (relative to the wild-type enzyme) were observed during nicotine coordination by CYP2A13.6 (Fig. 6B). In contrast, the Arg494Cys substitution present in CYP2A13.6 resulted in widening of its solvent channel (Fig. 6C). CYP2A13.9 follows the same trend, and substrate-dependent differences in CYP2A13.6 and CYP2A13.9 activities could stem from different 3D structures imposed by different interacting substrates. The coumarin 7-hydroxylation and NNK α -hydroxylation CL_{int} values for CYP2A13.9 expressed in *E. coli* decreased by 57% and 39%, respectively, relative to that for wild-type CYP2A13, whereas (S)-NNN 5'-hydroxylation CL_{int} values increased by 123% relative to that for wild-type CYP2A13. However, the CL_{int} values for several CYP2A13 variants were lower than that of wild-type CYP2A13 when evaluated using coumarin, NNK, and (S)-NNN [14]. Further studies using additional substrates such as tobacco-specific nitrosamines are needed to confirm the substrate-dependent differences in the activities of CYP2A13 variants.

In conclusion, wild-type and 8 CYP2A13 variants were expressed in 293FT cells and their enzymatic activities were characterized *in vitro*. These data reveal several functional alterations of CYP2A13 allelic variants caused by genetic polymorphisms. In

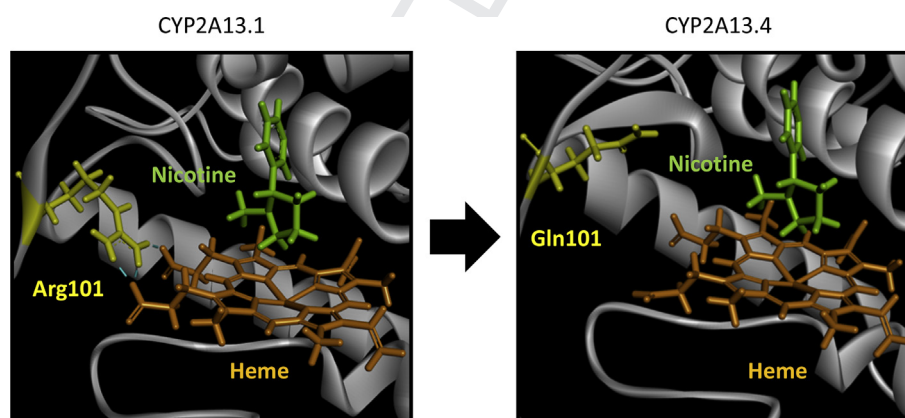


Fig. 4. Diagram of a portion of the crystal structure of CYP2A13.1 (left panel) and CYP2A13.4 (right panel). The residues Arg101 in CYP2A13.1 and Gln101 in CYP2A13.4 are shown in yellow. Heme is shown in orange. The interactions between Arg101 and heme are shown in light blue.

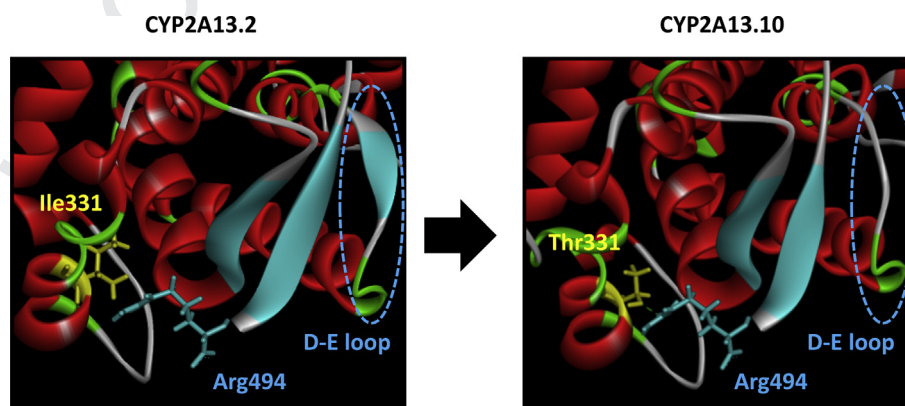


Fig. 5. Diagram showing a fragment of the crystal structures of CYP2A13.2 (left panel) and CYP2A13.10 (right panel). α -Helices and β -strands are shown in red and light blue, respectively. Ionic bonding was found to differ between CYP2A13.2 (Arg25Gln, Arg257Cys) and CYP2A13.10 (Arg25Gln, Arg257Cys, Ile331Thr).

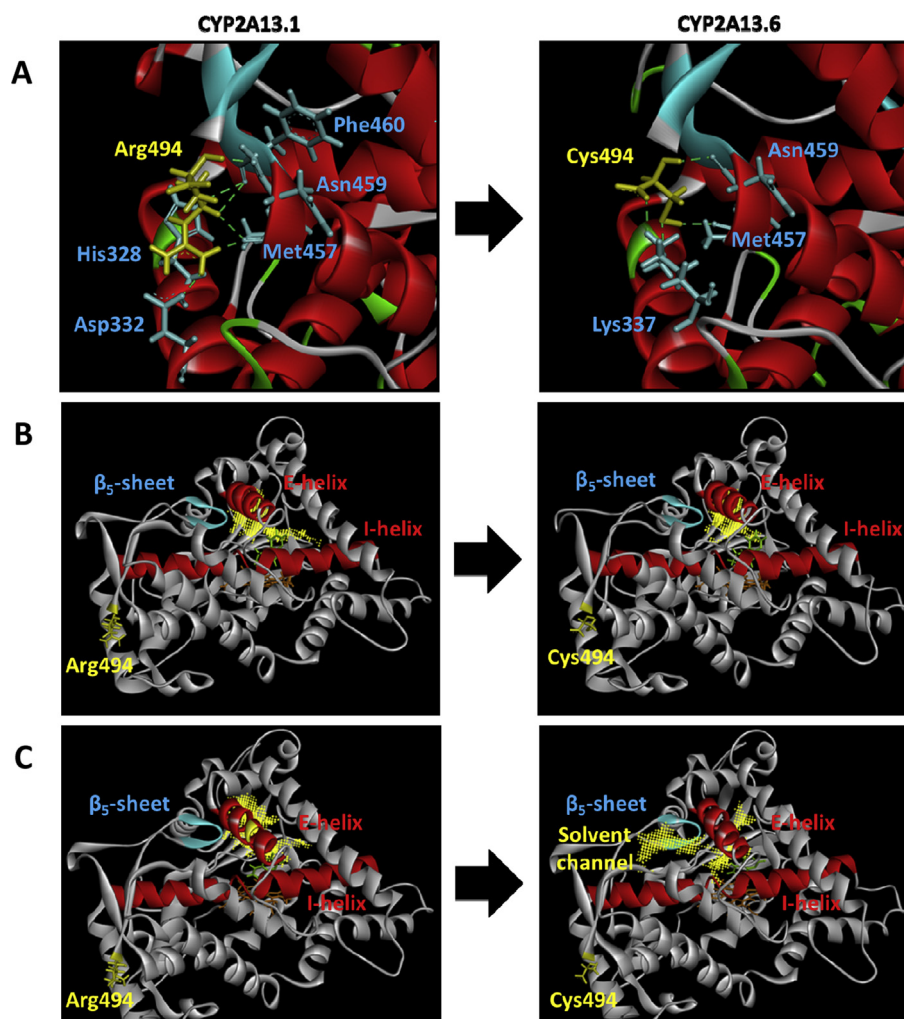


Fig. 6. Diagram showing a fragment of the crystal structures of CYP2A13.1 (left panel) and CYP2A13.6 (right panel). The residues Arg494 in CYP2A13.1 and Cys494 in CYP2A13.6 are shown in yellow (A). Hydrogen binding shown in light green was found to differ between wild-type CYP2A13 and CYP2A13.6. Diagram showing a fragment of the crystal structures of CYP2A13.1 and CYP2A13.6 complexed with nicotine (B) and coumarin (C). α -Helices and β -strand are shown in red and light blue, respectively. The channels are represented by the cluster in yellow.

particular, alteration of nicotine C-oxidation activity caused by CYP2A13 allelic variants was demonstrated for the first time. CYP2A13 is an important P450 isoform involved in bioactivation of several procarcinogens, including NNK, as well as nicotine and coumarin metabolism. These findings provide mechanistic insights underlying inter-individual differences associated with genotoxicity and cancer susceptibility.

Conflict of interest

The authors declare no conflict of interest.

Acknowledgements

We thank the Biomedical Research Core of Tohoku University Graduate School of Medicine for their technical support. We warmly thank Evelyn Marie Gutierrez, Tohoku University, for proofreading the manuscript.

Appendix A. Supplementary data

Supplementary data related to this article can be found at <https://doi.org/10.1016/j.dmpk.2017.11.004>.

References

- [1] Hecht SS. Biochemistry, biology, and carcinogenicity of tobacco-specific N-nitrosamines. *Chem Res Toxicol* 1998;11:559–603.
- [2] Bao Z, He XY, Ding X, Prabhu S, Hong JY. Metabolism of nicotine and cotinine by human cytochrome P450 2A13. *Drug Metab Dispos* 2005;33:258–61.
- [3] Murphy SE, Raulinaitis V, Brown KM. Nicotine 5'-oxidation and methyl oxidation by P450 2A enzymes. *Drug Metab Dispos* 2005;33:1166–73.
- [4] Uehara S, Uno Y, Inoue T, Sasaki E, Yamazaki H. Substrate selectivities and catalytic activities of marmoset liver cytochrome P450 2A6 differed from those of human P450 2A6. *Drug Metab Dispos* 2015;43:969–76.
- [5] Su T, Bao ZP, Zhang QY, Smith TJ, Hong JY, Ding XX. Human cytochrome p450 CYP2A13: predominant expression in the respiratory tract and its high efficiency metabolic activation of a tobacco-specific carcinogen, 4-(methylnitrosamino)-1-(3-pyridyl)-1-butanone. *Cancer Res* 2000;60:5074–9.
- [6] Ibuki Y, Shikata M, Toyooka T. gamma-H2AX is a sensitive marker of DNA damage induced by metabolically activated 4-(methylnitrosamino)-1-(3-pyridyl)-1-butanone. *Toxicol In Vitro* 2015;29:1831–8.
- [7] Zhang Z, Yang X, Wang Y, Wang X, Lu H, Zhang X, et al. Cytochrome P450 2A13 is an efficient enzyme in metabolic activation of aflatoxin G1 in human bronchial epithelial cells. *Arch Toxicol* 2013;87:1697–707.
- [8] Nakajima M, Itoh M, Sakai H, Fukami T, Katoh M, Yamazaki H, et al. CYP2A13 expressed in human bladder metabolically activates 4-aminobiphenyl. *Int J Cancer* 2006;119:2520–6.
- [9] Fujieda M, Yamazaki H, Kiyotani K, Muroi A, Kunitoh H, Dosaka-Akita H, et al. Eighteen novel polymorphisms of the CYP2A13 gene in Japanese. *Drug Metab Pharmacokinet* 2003;18:86–90.
- [10] Cauffiez C, Lo-Guidice JM, Quaranta S, Allorge D, Chevalier D, Cenee S, et al. Genetic polymorphism of the human cytochrome CYP2A13 in a French

- population: implication in lung cancer susceptibility. *Biochem Biophys Res Commun* 2004;317:662–9.
- [11] Tamaki Y, Honda M, Muroi Y, Arai T, Sugimura H, Matsubara Y, et al. Novel single nucleotide polymorphism of the CYP2A13 gene in Japanese individuals. *Drug Metab Pharmacokinet* 2011;26:544–7.
- [12] Kumondai M, Hosono H, Oriksa K, Arai Y, Arai T, Sugimura H, et al. CYP2A13 genetic polymorphisms in relation to the risk of bladder cancer in Japanese smokers. *Biol Pharm Bull* 2016;39:1683–6.
- [13] Zhang X, Su T, Zhang QY, Gu J, Caggana M, Li H, et al. Genetic polymorphisms of the human CYP2A13 gene: identification of single-nucleotide polymorphisms and functional characterization of an Arg257Cys variant. *J Pharmacol Exp Ther* 2002;302:416–23.
- [14] Schlicht KE, Michno N, Smith BD, Scott EE, Murphy SE. Functional characterization of CYP2A13 polymorphisms. *Xenobiotica* 2007;37:1439–49.
- [15] Wang H, Tan W, Hao B, Miao X, Zhou G, He F, et al. Substantial reduction in risk of lung adenocarcinoma associated with genetic polymorphism in CYP2A13, the most active cytochrome P450 for the metabolic activation of tobacco-specific carcinogen NNK. *Cancer Res* 2003;63:8057–61.
- [16] Wang SL, He XY, Shen J, Wang JS, Hong JY. The missense genetic polymorphisms of human CYP2A13: functional significance in carcinogen activation and identification of a null allelic variant. *Toxicol Sci* 2006;94:38–45.
- [17] Goto T, Moriuchi H, Fu X, Ikegawa T, Matsubara T, Chang G, et al. The effects of single nucleotide polymorphisms in CYP2A13 on metabolism of 5-methoxypsoralen. *Drug Metab Dispos* 2010;38:2110–6.
- [18] Omura T, Sato R. The carbon monoxide-binding pigment of liver microsomes. I. Evidence for its hemoprotein nature. *J Biol Chem* 1964;239:2370–8.
- [19] Guengerich FP, Martin MV, Sohl CD, Cheng Q. Measurement of cytochrome P450 and NADPH-cytochrome P450 reductase. *Nat Protoc* 2009;4:1245–51.
- [20] Omura T, Takesue S. A new method for simultaneous purification of cytochrome b5 and NADPH-cytochrome c reductase from rat liver microsomes. *J Biochem* 1970;67:249–57.
- [21] Nakajima M, Yamamoto T, Nunoya K, Yokoi T, Nagashima K, Inoue K, et al. Role of human cytochrome P4502A6 in C-oxidation of nicotine. *Drug Metab Dispos* 1996;24:1212–7.
- [22] Hosono H, Kumondai M, Maekawa M, Yamaguchi H, Mano N, Oda A, et al. Functional characterization of 34 CYP2A6 allelic variants by assessment of nicotine C-oxidation and coumarin 7-hydroxylation activities. *Drug Metab Dispos* 2016.
- [23] Ho MK, Mwenifumbo JC, Zhao B, Gillam EM, Tyndale RF. A novel CYP2A6 allele, CYP2A6*23, impairs enzyme function in vitro and in vivo and decreases smoking in a population of Black-African descent. *Pharmacogenet Genomics* 2008;18:67–75.
- [24] DeVore NM, Meneely KM, Bart AG, Stephens ES, Battaile KP, Scott EE. Structural comparison of cytochromes P450 2A6, 2A13, and 2E1 with pilocarpine. *FEBS J* 2012;279:1621–31.
- [25] Lewis DF. The CYP2 family: models, mutants and interactions. *Xenobiotica* 1998;28:617–61.
- [26] Lehnerer M, Schulze J, Achterhold K, Lewis DF, Hlavica P. Identification of key residues in rabbit liver microsomal cytochrome P450 2B4: importance in interactions with NADPH-cytochrome P450 reductase. *J Biochem* 2000;127:163–9.
- [27] Kobayashi K, Takahashi O, Hiratsuka M, Yamaotsu N, Hirono S, Watanabe Y, et al. Evaluation of influence of single nucleotide polymorphisms in cytochrome P450 2B6 on substrate recognition using computational docking and molecular dynamics simulation. *Plos One* 2014;9.
- [28] Hadidi H, Zahlsen K, Idle JR, Cholerton S. A single amino acid substitution (Leu160His) in cytochrome P450 CYP2A6 causes switching from 7-hydroxylation to 3-hydroxylation of coumarin. *Food Chem Toxicol* 1997;35:903–7.
- [29] Ghosh D, Jiang W, Lo J, Egbuta C. Higher order organization of human placental aromatase. *Steroids* 2011;76:753–8.
- [30] Cojocaru V, Winn PJ, Wade RC. The ins and outs of cytochrome P450s. *Biochim Biophys Acta* 2007;1770:390–401.